JOURNAL OF AIRCRAFT
Vol. 30, No. 6, Nov.–Dec. 1993

Prediction of Fluctuating Pressure in Attached and Separated Turbulent Boundary-Layer Flow

A. L. Laganelli*
Science Applications International Corporation, Fort Washington, Pennsylvania 19034
and
H. F. Wolfe†
WL/FIBG, Wright-Patterson Air Force Base, Ohio 45433

A methodology is presented that predicts the fluctuating pressure and power spectra for attached zero-pressure gradient and separated turbulent boundary-layer flow on smooth and rough surfaces. Attached flow conditions use a prediction technique that employs a transformation of boundary-layer properties from the compressible to the incompressible plane where a comparison can be made to an extensive data base. For a rough wall, it is shown that the rms pressure, which scales with wall shear, can be predicted by augmenting the smooth wall value by the rough/smooth skin-friction ratio. Relative to nonattached flow, represented by two-dimensional compression corner and three-dimensional fin-generated shock/boundary-layer interactions, the rms pressure is shown to scale with approach flow conditions and the oblique shock inviscid pressure rise. For this situation, a new inviscid angle has been defined as $\phi = \alpha + \beta \sin^{-1}(1/M)$ where α is the shock generator angle and β is a parameter based on two-dimensional or three-dimensional interactions. Both rms pressure and power spectra have been correlated in terms of undisturbed approach flow boundary-layer parameters and modified inviscid shock strength relations to provide engineering solutions for the design resolution to complex flow problems.

Nomenclature

A = parameter, Eq. (9)
b = compressibility exponent, Eq. (15)
C_f = skin-friction coefficient
C_p, $\bar{C}_p$ = pressure coefficient, $(P - P_1)/q_1$
F_c = transformation function, Eq. (7)
f, ω = frequency
h = enthalpy
K = parameter, Eq. (2)
k' = parameter, Eqs. (2) and (4)
l = characteristic length
M = Mach number
P_w = local boundary-layer static pressure
$\bar{p}$ = rms fluctuating pressure
q = dynamic pressure, $(\gamma/2)PM^2$
Re = Reynolds number
r = turbulent recovery factor, 0.896
t = time
u, v = velocity in stream and normal directions
V = characteristic velocity
x, y = coordinate distance in stream and spanwise direction, respectively
α = shock generator angle
β = correction to swept shock, Eq. (26)
γ = ratio of specific heats, 1.4 for air
δ^* = boundary-layer displacement thickness
θ_s = oblique shock angle
λ = parameter, viscous/velocity power law exponent, Eq. (8)
τ = shear stress
ϕ = shock angle based on swept shock/boundary-layer interaction, Eq. (26)
$\phi(\omega)$, $\phi(f)$ = power spectral density

Subscripts
aw = adiabatic wall
c = compressible conditions or swept corner angle
e = evaluated at edge of boundary layer
i = incompressible conditions
s = reference to calculated inviscid shock position
x = based on wetted length, axial length
w = wall
0 = reference condition, smooth wall
1 = approach flow upstream of interaction
2 = shock/boundary-layer interaction region, peak, plateau
∞ = freestream conditions

Superscript
* = reference temperature condition

Presented as Paper 89-1064 at the AIAA 12th Aeroacoustic Conference, San Antonio, TX, April 10–12, 1989; received March 6, 1991; revision received Dec. 11, 1992; accepted for publication Jan. 29, 1993.

*Chief Scientist, Assistant Vice President, Fluid and Propulsion Sciences Operation. Member AIAA.
†Technical Manager, Acoustic/Sonic Fatigue. Associate Fellow AIAA.

Introduction

THE high temperatures and fluctuating pressures experienced in hypersonic turbulent boundary-layer flows are a primary design consideration as a result of their impact on dynamic and strength characteristics of vehicle structures. In addition to potential structural failure, the turbulent-induced aeroacoustic excitations can cause unacceptable sound pressure levels to equipment stations on the vehicle, as well as the crew compartment on manned vehicles. Lifting bodies that utilize control surfaces generate higher sound pressure levels as a result of the increased static pressure, as well as the potential for separated flow regions. Hence, a fundamental knowledge of hypersonic flow and associated material characteristics, structural design, and fatigue in terms of coupled thermal-vibro-acoustic behavior is required. Paramount to structural fatigue analysis is the prediction of the aero-

acoustics loads which are directly related to mission profiles (trajectory).

Empirical models have been developed to predict aeroacoustic loads on hypersonic structures that have been based on ground test data and limited flight data for axisymmetric[1] as well as three-dimensional maneuvering bodies,[2] where both ground and flight measurements show high vibration levels that were attributed to flow interactions associated with control surfaces.

The algorithms developed to date have generally evolved from shapes ($M >> 1$) that are planar, two-dimensional, or axisymmetric, except for control surface regions. Moreover, the algorithms, which were developed from physical laws, are generally for attached turbulent boundary-layer flows. Regions experiencing flow separation present a much more complex flow structure for modeling. Future hypersonic vehicles will require lifting body configurations where vehicle lengths are an order of magnitude longer than many of the configurations from which aeroacoustic predictive techniques were developed. Figure 1 shows a typical hypersonic configuration featuring three-dimensional noncircular cross sections with ramps, control surfaces, and shock/boundary-layer interactions.

Reference 3 represents a review of the state of the art of aeroacoustic loads prediction techniques of supersonic/hypersonic conditions for attached turbulent boundary-layer flow. This work was extended[4] to high Reynolds number flows and added surface roughness effects while Ref. 5 considers coupled surface roughness and blowing. Relative to flow interaction phenomena for steady and unsteady flows, Settles and Dowling[6] provide a review of swept shock wave/boundary-layer interactions, including a classification of flow regimes. As a result of the complex three-dimensional nonlinear interaction, experiments have led the way to investigate the interaction phenomena due to restrictive assumptions and limitations in analysis. Reference 6 also reviews the experimental work generated at Princeton University of which Refs. 7–12 represent a partial list which will be the basis of developing acoustic algorithms for shock/boundary-layer interactions in the present investigation.

Since the original development of this work, a significant data base has been generated at Mach 5 conditions. This data base includes swept/unswept compression corner interaction (primarily at a ramp angle of 28 deg) and three-dimensional fin-generated shock interactions. Refs. 13 and 14 provide a tracking of these results. Experiments were also conducted for cylinder-induced shock interactions.[15] The regions associated with swept shock/boundary-layer interaction have been described by Settles and Dolling.[16]

The work reported herein has attempted to develop an engineering technique to predict the peak acoustic loads associated with the intermittent region of compression ramps and fin-generated shock/boundary-layer interactions. While the original work[17] focused on the available data base ($M \leq 3$) to develop correlations, the present work considers recent data at Mach 5 to determine compressible effects as well as substantiate the techniques developed at Mach 3.

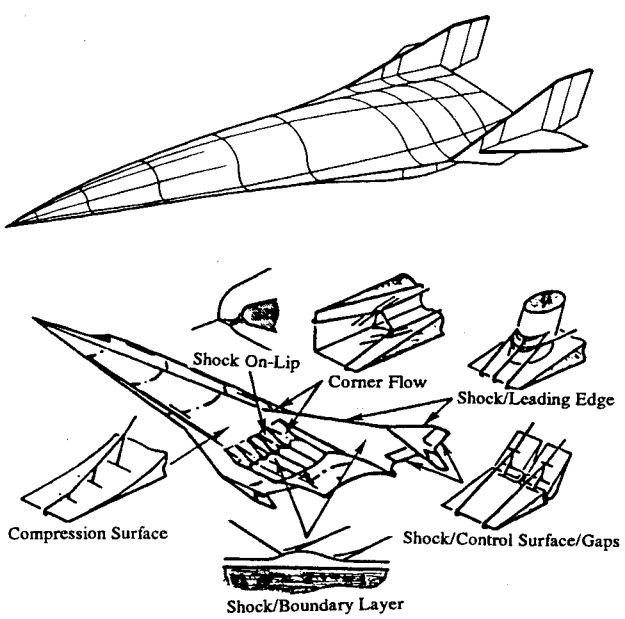

Fig. 1 Hypersonic space transportation system with flow interaction regimes.

Discussion

Attached Zero Pressure Gradient Flow Algorithms

A review of prediction methods to characterize rms pressure fluctuations in attached turbulent boundary-layer flows have been found to scale with the boundary-layer dynamic pressure, Mach number, and wall temperature ratio. Generally, power spectral density (PSD) and rms pressure ($\tilde{p}$) were developed independently from experimental evidence. The following will relate the two functions using definitions of power spectra with the Houbolt algorithm.[3] Compressibility and heat transfer of the medium will be incorporated, as well as boundary-layer profile, boundary-layer growth, and viscous effects. The development is based on experimental data as well as fluid dynamic principles.

The PSD can be generalized as a function of the spectrum as

$$\phi(\omega) = \frac{\phi(0)}{1 + K^2\omega^2} \tag{1}$$

where K represents an attenuation in the PSD profile[2] to be compliant with the flow medium. K is dependent upon the properties of the flow, namely

$$K = k'l/V \tag{2}$$

with k' to be defined. Using the definition of rms pressure $(\tilde{p})^2 = \int^{\infty} \phi(\omega)\, d\omega$ together with Eq. (1), there results

$$\left(\frac{\tilde{p}}{q}\right)^2 = \frac{\phi(0)\pi/2}{k'(l/V)q^2} \tag{3}$$

where normalization was made with the dynamic pressure $[q = P(\gamma/2)M^2]$ based on boundary-layer edge conditions.

Equations (1) and (3) can then be written as

$$\frac{\phi(\omega)V}{q^2 l} = \frac{(\tilde{p}/q)^2 k'(2/\pi)}{1 + [k'(l/V)\omega]^2} \tag{4}$$

which is recognized as the familiar format for representing PSD in the literature. The characteristic length is generally chosen as the boundary-layer displacement thickness, while the characteristic velocity as the boundary-layer edge value u_e. Laganelli[2] noted that k' appeared to have physical interpretation representing compressibility and heat transfer of the fluid medium. This was a consequence of the magnitude of the PSD as $\omega \to 0$, as well as the rolloff of the PSD as $\omega \to 10^4$ Hz ($f > 2000$ Hz, i.e., $\omega = 2\pi f$).

If one considers the low frequency ($\omega \to 0$) regime, Eq. (4) becomes

$$\frac{\phi(\omega \to 0)V}{q^2 l} \to \left(\frac{\tilde{p}}{q}\right)^2 k' \frac{2}{\pi} \tag{5}$$

Solutions are obtained using the algorithm developed in Ref. 3 for rms pressure

$$\tilde{p}/q = 0.003AF_c^{\lambda} \tag{6}$$

where A is a parameter to be defined and F_c is a transformation function from compressible/incompressible flow states, namely

$$F_c = \frac{C_{fi}}{C_{fc}} = \frac{h^*}{h_e} = \frac{1}{2} + \frac{h_w}{h_{aw}}\left(\frac{1}{2} + r\frac{\gamma - 1}{4}M_e^2\right) + 0.22r\frac{\gamma - 1}{2}M_e^2 \tag{7}$$

$$\lambda + [2m - (1 + n)]/(3 + n) \tag{8}$$

where n and m are velocity $[u/u_e = (y/\delta)^{1/n}]$ and viscosity $[\mu/\mu_e = (T/T_e)^m]$ power law exponents, respectively. For incompressible flow, $F_c \rightarrow$ unity and $A \rightarrow 2$ such that $(\tilde{p}/q)_i \rightarrow 0.006$, a value that, while accepted by the scientific community, is believed to be in error[10] as a result of instrumentation gauge size limitations. The errors could yield incompressible values of $(\tilde{p}/q)_i \rightarrow 0.010$. Until this question is resolved, the value 0.006 will be used.

In order to determine the characteristics of A, an inspection of Eq. (5) is made using Eq. (6), namely

$$\frac{\phi(\omega \rightarrow 0)V}{q^2 l} \rightarrow 5.73 \times 10^{-6}A^2 k' F_c^{2\lambda}$$

By allowing $k' = F_c^{-2\lambda}$ to match the rolloff for $\omega >> 1$ as provided by data, A cannot be constant since the normalized PSD is not constant with the compressibility and heat transfer of the flow medium. This suggests $A = A(F_c)$, let

$$A = 2F_c^{\lambda b} \tag{9}$$

where b is some arbitrary value that also has been shown to have physical meaning and allows for the interpretation between rms pressure and PSD.

Consider the following definition[5] for transforming the compressible flow state to incompressible conditions where acoustic algorithms can be validated with a more extensive data base. Let

$$\tilde{p}/\tau_w = \text{parameter} = A \tag{10}$$

and define

$$F_A = \frac{A_i}{A_c} = \frac{(\tilde{p}/q)_i C_{fc}}{(\tilde{p}/q)_c C_{fi}} = \frac{0.006}{(\tilde{p}/q)_c}\frac{1}{F_c} \tag{11}$$

Data has shown that $(\tilde{p}/q)_c$ is a weak function of Reynolds number, but a strong function of compressibility and heat transfer of the medium. If F_A is unity, the above becomes

$$(\tilde{p}/q)_c = 0.006/F_c \tag{12}$$

and for adiabatic wall conditions [using Eq. (7)]

$$(\tilde{p}/q)_{c,aw} = 0.006/(1 + 0.13M_e^2) \tag{13}$$

which is recognized as the Lowson[18] algorithm.

Allowing for the new definition of A, Eq. (9), to be used with Eq. (6), results in the expression

$$\tilde{p}/q = 0.006F_c^{\lambda(1+b)} \tag{14}$$

Moreover, for F_A = unity, a comparison of Eqs. (15) and (12) suggests that $\lambda(1 + b) = -1$ which leads to a definition of "b" as follows:

$$b = 2(m + 1)/[(1 + n) - 2m] \tag{15}$$

Using realistic values of velocity power law exponent ($7 \leq n \leq 12$) together with viscous power law exponent ($0.6 < m < 1.0$), values of b fall in the range $0.3 < b < 0.6$ which are consistent with values experimentally determined in Refs. 2 and 3 in the range $0.3 < b < 0.5$. It should be noted that for values of $m = 0.7$, $n = 9$, and $b = 0.4$, Eq. (15) becomes $\tilde{p}/q \rightarrow 0.006/F_c$.

Equations (14) and (5) provides the PSD which can be written as

$$\frac{\phi(\omega)V}{q^2 l} = 2.293 \times \frac{10^{-5}F_c^{-0.5733}}{\{1 + F_c^{2.867}[(l/V)\omega]^2\}} \tag{16}$$

As $\omega \rightarrow 0$

$$\frac{\phi(\omega \rightarrow 0)V}{q^2 l} \rightarrow 2.293 \times 10^{-5}F_c^{-0.5733} \tag{17}$$

Rough Surface

Analytical and experimental investigations have shown the surface shear characteristics (hence acoustic loads) to be augmented in the presence of rough surfaces.[4] The normalized rms pressure [Eq. (10)], which has been shown[19,20] to be applicable for smooth and rough surfaces, can be expressed as

$$(\tilde{p}/q)_c = AC_f = AC_{f_0}(C_f/C_{f_0}) \tag{18}$$

Equation (14) becomes

$$(\tilde{p}/q)_c = 0.006F_{c_0}^{\lambda(1+b)}(C_f/C_{f_0}) \tag{19}$$

The normalized rms pressure can be obtained from Eq. (10) together with Eqs. (18) and (19), using the Blasius form for drag, such that

$$\tilde{p}/\tau_\omega = (\tilde{p}/q)(q/\tau_\omega) = 0.003F_{c_0}^{\lambda b}Re_x^{[2/(3+n_0)]}/k(n_0) \tag{20}$$

In Eq. (20), the parameters on the right side of the equation reflect smooth wall conditions. For fixed Reynolds number, the normalized shear is a function of the compressibility and heat transfer of the medium (F_{c0}) which, in turn, is fixed for a given tunnel condition, thereby satisfying the condition of Eq. (10). The sole effect of roughness on rms fluctuating pressure and wall shear stress is expressed through the skin friction relation, C_f/C_{c0}, as noted in Eq. (18). Reference 4 provides for the PSD on a rough surface compared to measured data using Eqs. (16) and (18), respectively.

Shock/Boundary-Layer Interaction Flows (Nonattached)

Spanwise propagation of inboard corner boundary conditions and subsequent shock/boundary-layer interaction have become an issue in high-speed aircraft design. The problem has been enhanced by the interaction of unsteadiness that result in a fluctuating pressure field that impacts the structural response and fatigue life. The limitation of a data base has hampered the development of engineering models to describe this phenomena for mean flows and is further restricted for unsteady type interactions.

Compression Corner

The two-dimensional compression corner provides an excellent geometry to investigate shock/boundary-layer behavior since this type of configuration has received significant attention in the literature. However, fluctuating pressure and associated spectra has been limited in Mach number range ($\leq$5). Shock/boundary-layer characteristics of flow over compression ramps[6,12,16,21-23] show the mean pressure distribution to rise upstream of the corner creating a flow separation region (subsonic) that reattaches on the ramp. The extent of this region and the strength of the shock is dependent upon

the angle of deflection of the ramp (α). Above the separation region, a wave system is developed that coalesces into a single shock.

The unsteadiness of this type of interaction is characterized by two peak positions relative to the points of flow separation and reattachment. The maximum peak value located at approximately $2\delta_0$ upstream of the corner is characteristic of shock oscillations observed in other experiments experiencing two-dimensional flow separation.

The work of Ref. 21 was extended by Dolling and Or[12] to include the effects of shock strength (ramp angle), while Tran[7] investigated the geometric effects of generating the shock with swept corner interaction. Figure 2 shows the fluctuating pressure, normalized by local static wall pressure, for the various ramp angles tested in Ref. 12. A decrease in normalized rms fluctuating peak pressure, as well as plateau levels, is experienced with decreasing shock strength. It is interesting to note that the lowest ramp angle while displaying attached flow characteristics still has a rise in the rms fluctuating peak level.

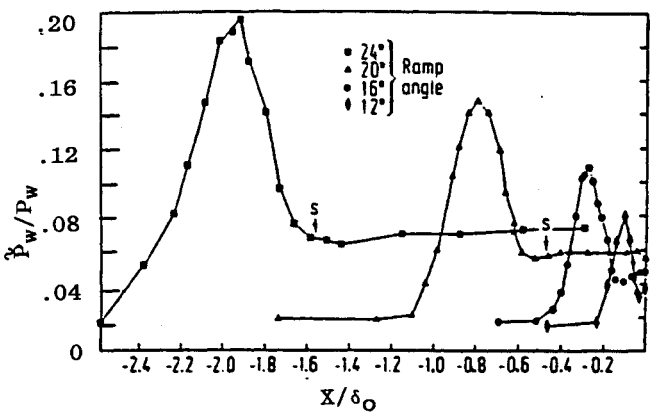

Fig. 2 Root-mean-square pressure distribution with shock strength (two-dimensional interaction).[12]

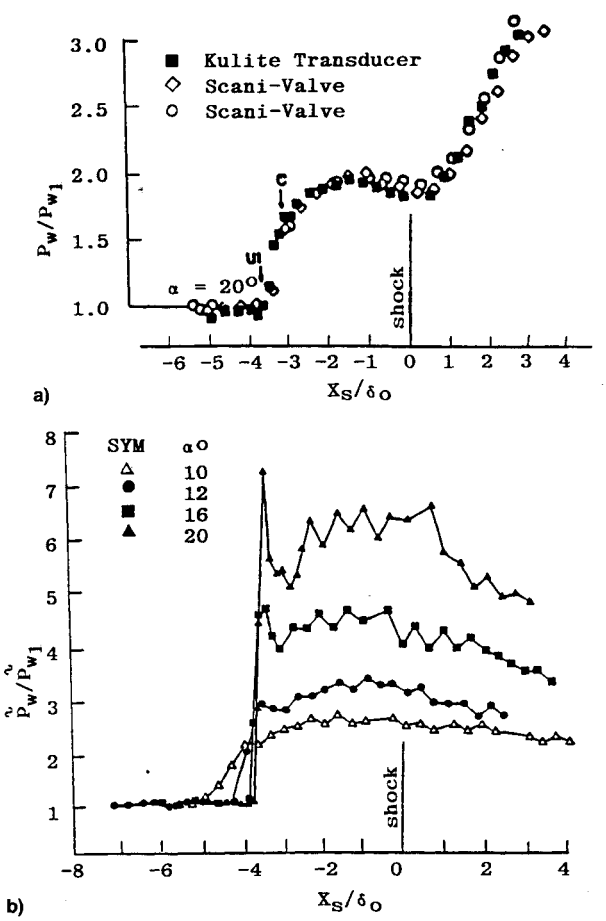

Fig. 3 Fin-generated (three-dimensional) shock/boundary-layer interactions for a) mean and b) fluctuating pressure.[23,24]

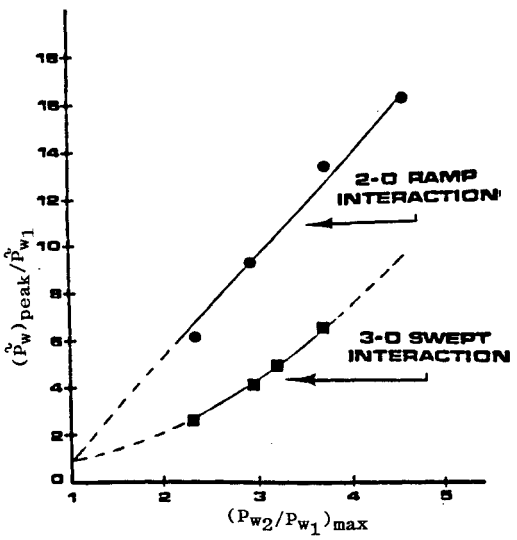

Fig. 4 Peak rms pressure variations for two-dimensional/three-dimensional interaction with shock strength.[7]

Fin-Generated Shock/Boundary-Layer Interactions

Tran[7] conducted an investigation that focused on unsteadiness in fin-generated shock layer/turbulent boundary-layer interaction while comparing the results to the two-dimensional compression corner interactions.[9,23,24] It was shown that the two-dimensional (compression corner) and fin-generated shock/boundary-layer interactions, while providing similar characteristics, were inherently different as a result of the response to the same approach flow.

Figure 3 shows the results of the various sharp fin-generated interactions for both mean and fluctuating pressure. In Fig. 3a, the mean distribution shows locations for the upstream influence (UI) and coalescence (C) line where the latter is the location of flow separation. The UI line corresponds to the position of initial pressure rise, while the coalescence line does not appear to relate with any flow feature of the mean distribution. Both mean pressure (20-deg fin data shown) and rms pressure show a dependence on shock strength as experienced in the two-dimensional ramp experiments. However, the rms peak for the three-dimensional swept interaction appears to be approximately one-half the value experienced in the two-dimensional rms pressure rise for similar approach flow and similar shock strength. Also, the rms fluctuating pressure peaks suggests an intermittent action at the start of the interaction, even though the mean pressure has not shown a significant increase.

A comparison of two-dimensional ramp and swept-type interactions was made by Tran,[7,9] based on the similar behavior at the start of the interaction. These interactions were compared to flow phenomena that showed strong dependence to the intermittent characteristics. This includes overall inviscid pressure rise, the peak rms fluctuating pressure, pressure gradient distribution, and spatial extent of large amplitude disturbance.

Figure 4 shows a comparison of the rms pressure subject to the above noted flow characteristics for the two-dimensional ramp and three-dimensional fin-generated interactions. The rms peak increases with shock strength and magnitude and for a given inviscid pressure rise, the swept interaction is approximately half of that of the corresponding two-dimensional ramp interaction.

Correlation of rms Pressure—Interactive Flows

An examination of the normalized rms fluctuating pressure distributions for two-dimensional ramp (corner flow) and three-

dimensional fin-generated shock interactions show a peak occurrence and plateau region prior to reducing to the approach flow levels. The development of the acoustic load algorithms for shock/boundary-layer interactions will focus on these regions with consideration to flow behavior of the mean properties of the interaction. Moreover, the predictive technique will incorporate the approach flow characteristics, where algorithms have been developed, which have been shown to relate to the interaction phenomena.

Data suggests that the peak rms fluctuating pressure level occurs prior to separation and rapidly reduced to the plateau level. This level appears to be related to the magnitude of the initial pressure gradient and spatial extent of the gradient.[7] However, in the plateau region, the effect of the pressure gradient or its spatial extent does not appear to be sensitive (for the Mach 3 data base), hence, a correlation relating the approach flow and shock strength will be attempted, namely

$$(\tilde{P}_{W_2}/P_{W_2})_{\text{plat}} \simeq (\tilde{P}_{W_1}/P_{W_1})(P_{W_2}/P_{W_1})_{\max} \tag{21}$$

With consideration to Eq. (14), the rms pressure for the approach flow can be written as

$$(\tilde{P}_{W_1}/P_{W_1}) \simeq 0.006(\gamma/2)M_1^2 F_c^{\lambda(1+b)} \tag{22}$$

where the dynamic pressure $[q_1 = (\gamma/2)P_1M_1^2]$ was used.

Let $\tilde{p}/q \rightarrow 0.006/F_c$ (i.e., $n = 7$, $m = 0.8$, and $b = 0.4$) at adiabatic wall conditions, the approach flow can be expressed as

$$\left(\frac{\tilde{P}_{W_1}}{P_{W_1}}\right)_{\text{approach}} = \frac{0.006(\gamma/2)M_1^2}{1 + 0.13M_1^2} \tag{23}$$

where for $M_1 \simeq 3$, $\tilde{P}_{W_1}/P_{W_1} \simeq 0.0174$ which compares with the results of Fig. 2. The maximum inviscid pressure rise (shock strength) is obtained from the oblique shock relation

$$\left(\frac{P_{W_2}}{P_{W_1}}\right)_{\max} = \frac{2\gamma M_1^2 \sin^2\theta_s - (\gamma - 1)}{\gamma + 1} \tag{24}$$

where θ_s is approximated[3] by

$$\theta_s \simeq \alpha + \sin^{-1}(1/M_1) \tag{25}$$

for α the shock generator angle.

For the two-dimensional corner flow at a ramp angle of 24 deg, the maximum inviscid pressure rise becomes $(P_{W_2}/P_{W_1})_{\max} \simeq 4.6$ such that the normalized fluctuating pressure [Eq. (21)] has a value of 0.080, which shows good agreement with the results of Fig. 2. On a 16-deg ramp, the normalized fluctuating pressure in the plateau region has a value of 0.0552 which also shows good comparison to Fig. 2.

When comparing the predictive technique for fluctuating pressure levels generated by three-dimensional fin-generated swept shock/boundary-layer interactions, the technique overpredicts the experimental results. Accordingly, the flowfield structure was re-examined relative to mean flow and wall (heat transfer/shear) characteristics to determine the variation in the inviscid pressure rise. Figure 5 shows the basic characteristic of a three-dimensional swept shock interaction of a fin/plate where the fin is mounted on the plate as described by Neumann and Hayes,[25] using oil flow tracings of the three-dimensional interaction together with surface pressure and heat transfer data (a more extensive definition for spherical/polar coordinates is provided in Ref. 16). The pressure distribution is shown divided into two regions by the fin-generated oblique shock wave. An outer region extends from onset of the interaction to the shock wave, representing a region of separated flow (with sufficient shock strength). The flow in this region has distinct two-dimensional characteristics. The inner region is characterized by a sharp peak in pressure that lies close to the fin.

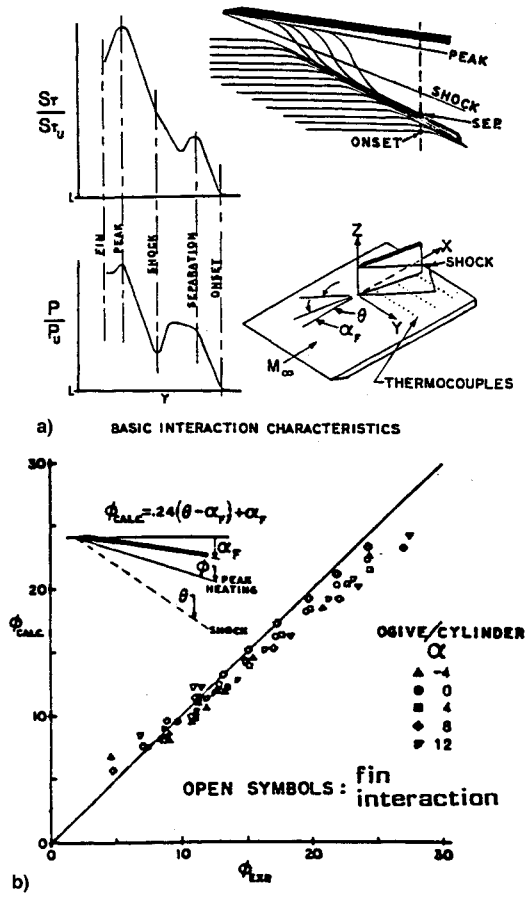

Fig. 5 Basic fin-generated shock/boundary-layer interaction with peak wall shear location[25]: a) basic interaction characteristics and b) peak heating (shear) location.

Peak pressure and heating occur along a divergent streamline close to the shock generator. Maximum streamline divergence occurs at the shock location as determined by oblique shock relations. The line of boundary-layer separation is observed to be the inner edge of the oil accumulation line, and onset is the point at which the undisturbed streamlines first begin to curve.

The location of peak mean pressure and heating occurs approximately along a streamline from the shock generator leading edge. The angle ϕ between this ray and the freestream direction has been correlated as $\phi = 0.24\,(\theta_s - \alpha) + \alpha$. In an attempt to coalesce the two-dimensional compression corner and three-dimensional fin-generated interaction data for peak rms pressure, in the intermittent region, a modified inviscid shock angle is introduced with an arbitrary constant (β), and is expressed as

$$\phi = \alpha + \beta \sin^{-1}(1/M) \tag{26}$$

where

$$\left.\begin{array}{ll} \text{(i)} & \beta = \text{unity @ two-dimensional flow } (\phi = \theta_s) \\ & \text{peak rms fluctuating pressure} \\ \text{(ii)} & \tfrac{1}{2} < \beta < 1 \text{ @ rms peak fluctuating pressure} \\ & \text{for three-dimensional fin-generated shock/} \\ & \text{boundary-layer interactions that will be de-} \\ & \text{fined with the data base} \end{array}\right\} \tag{27}$$

The modified shock angle can then be applied to the inviscid oblique shock pressure relationship [Eq. (24)] to correlate the peak rms pressure in the intermittent regime.

With reference to Fig. 4, the normalized peak rms fluctuating pressure for a two-dimensional/three-dimensional shock/boundary-layer interaction is correlated as (Fig. 6)

$$(\tilde{P}_W/\tilde{P}_{W_1})_{\text{peak}} = -1.181 + 1.713(P_{W_2}/P_{W_1})_{\max,\phi} + 0.468(P_{W_2}/P_{W_1})^2_{\max,\phi} \quad (28)$$

for $P_{W_2}/P_{W_1} \geq 1$. The inviscid pressure rise is obtained using Eq. (24) with the new angle ϕ [Eq. (26)] at $\beta = 0.6$, which was determined from the $M \leq 3$ data base.

Relative to the plateau region of a three-dimensional fin-generated shock/boundary-layer interaction, Eq. (21) is used together with $\beta = 0.6$ in Eq. (26). An examination of the fin-generated data presented in Fig. 3 shows that the normalized rms plateau pressure has a value of 0.0452, for a fin angle $\alpha = 20$ deg, which is representative of the levels shown. Similar results are easily obtained for other fin angles which show good comparison to measured data.

An inspection of Eq. (24) would imply that the rms peak fluctuating pressure would continue to rapidly increase with increasing Mach number in separated flow regions. On the other hand, the rms pressure was shown to approach an asymptotic level with increasing Mach number for attached flow conditions [e.g., Eq. (13)]. Therefore, the data base at Mach 5, for two-dimensional ramps and three-dimensional fin-generated interactions, were added to Fig. 6. A value of $\beta = 0.6$ was used for the fin-generated interactions. Unfortunately, all the compression ramp data with and without a swept corner, were obtained with one ramp angle ($\alpha = 28$ deg). While the data did not collapse, comparable shock-generating angles ($\alpha = 20$ deg) for Mach 3 and 5 show the normalized peak rms pressure to decrease with increasing Mach number. Moreover, if the abscissa is normalized by M^2, the data would tend to coalesce, which would imply that the normalized peak rms pressure would scale with the sin ϕ, the new inviscid shock angle. This result is shown in Fig. 7 with the entire data base.

Correlations were attempted by Schmisseur and Dolling[13] using freestream pressure to normalize the peak rms pressure with sweep angle of the separation line. However, when the Dolling and Or[12] unswept compression ramp data was applied to the correlation, a considerable scatter in the data is experienced as the swept angle approaches zero. Other normalizing parameters could be used with the peak rms pressure, as well as variations in the inviscid oblique pressure rise equation, sweep angle, etc., however, the focus of this article has been to provide correlations for the design process of high-speed aerodynamic configurations. For this situation, compression ramps and fin-generating shock/boundary-layer interactions will be provided by small ($\alpha < 10$ deg for three-dimensional and $\alpha < 20$ deg for two-dimensional) shock-generating angles that will result in weaker interactions. Figure 7 shows that the ratio of peak rms pressure resulting from interactions to approach flow levels will be <10 for practical applications.

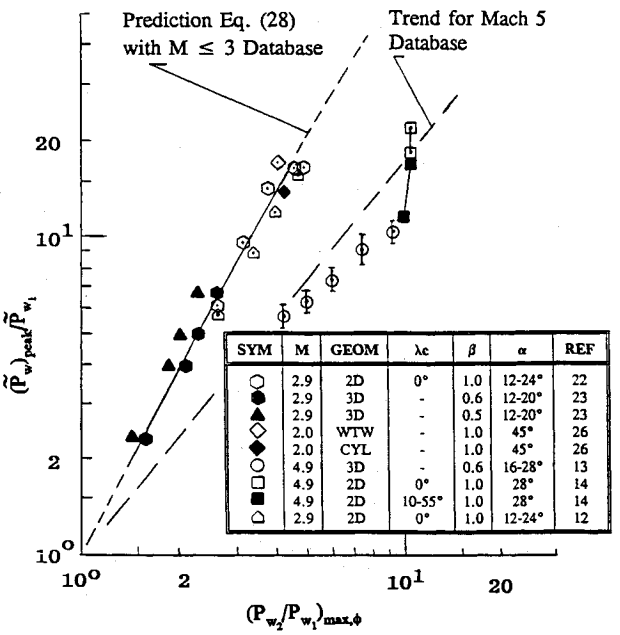

Fig. 6 Correlation of peak rms pressure for shock/boundary-layer interactions.

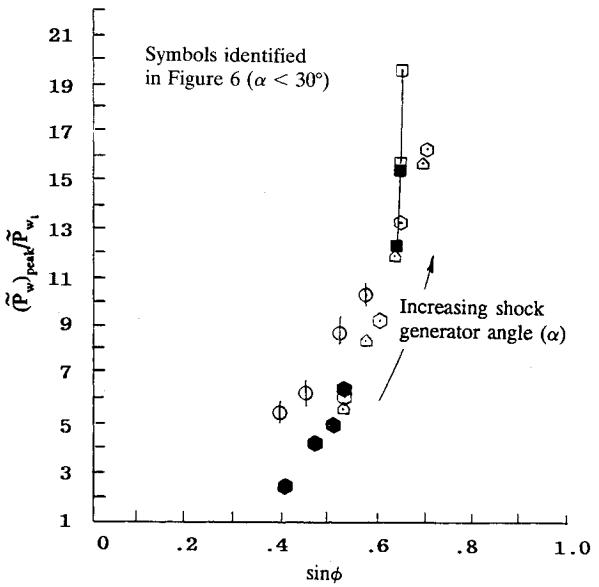

Fig. 7 Correlation of peak rms pressure with modified inviscid shock angle.

An exception to the above may occur for shock impingement on control surfaces (e.g., fuselage bow shock on cowl lip or on wings/stabilizers) or corner flow interactions (inlets on air breathing vehicles). Data will be required to assess these interactions. Moreover, data at extended Mach numbers ($M > 5$) will be required to determine the impact of hypersonic conditions on acoustic loads subject to flow separation.

Plateau Region Mean Pressure

Since it is difficult to define the location within the boundary layer to estimate the mean pressure rise associated with the plateau region of separated boundary-layer flow, the correlation of Nestler[27] is recommended for forward facing steps. This is expressed as

$$\frac{(P_p/P_{W_1}) - 1}{(\gamma/2)M_1^2} = \frac{4.7}{(M_1^5 Re_{x_1})^{0.148}} \quad (29)$$

Moreover, if one considers the pressure rise for an oblique compression shock together with Eq. (29), and compressible flow tables for shock separation angles over a range of Reynolds and Mach numbers, a value of $\theta_s \simeq 10$ deg is a representative average flow turning angle. For this condition, the mean pressure rise in the plateau region can be approximated by[27]

$$(P_{\text{plateau}}/P_{W_1}) \simeq [1 + (\gamma/2)\bar{C}_p M_1^2]^{0.8} \quad (30)$$

where $\bar{C}_p$ is the pressure coefficient based on a 10-deg ramp angle with approach flow Mach number M_1 (where one notes the elimination of the Reynolds number dependence.)

Swept shock/boundary-layer interactions (three-dimensional) were extensively investigated by Hayes and Neumann,[25] Holden,[28] and Scuderi[29] and reviewed in Ref. 27. It

is shown that the correlations given by Eqs. (29) and (30) are representative of the mean pressure data in the plateau level region for both two-dimensional and three-dimensional shock/boundary-layer interactions.

Correlation of Power Spectra—Interactive Flows

Power spectra characterizing shock/boundary-layer interactions has been investigated in early studies by Coe et al.[26] and Robertson,[30] as well as the recent work reported in Refs. 12, 22, and 24. An increase in the power spectra of the pressure fluctuations due to interaction phenomena is experienced above the attached flow level. While the spectra tend to converge toward a common level and slope at high frequencies, a significant variation exists between the separated flow spectra and that of the attached flow distribution. It was noted that the very low-frequency components of the fluctuating pressures are increased in intensity, while the intermediate and high-frequency retain the characteristics of the approach (attached) boundary layer. Approach flow boundary-layer parameters are generally selected for normalizing the power spectra as a matter of convenience, since local scale lengths and velocities in the interaction region are not well defined. Moreover, with consideration to engineering design requirements, it would be useful to develop prediction algorithms employing boundary-layer approach flow characteristics that are deterministic.

Figure 8 shows the compression corner results for a 24-deg ramp. For this case the PSD were not normalized. The approach flow displays a characteristic that is typical of power spectra that includes low frequency peaks associated with facility generated noise. A comparison is made to the present prediction technique. Figure 8b shows the spectra at several locations relative to the corner of the ramp. These do not show an indication of a frequency peak and tend to display broadband characteristics.

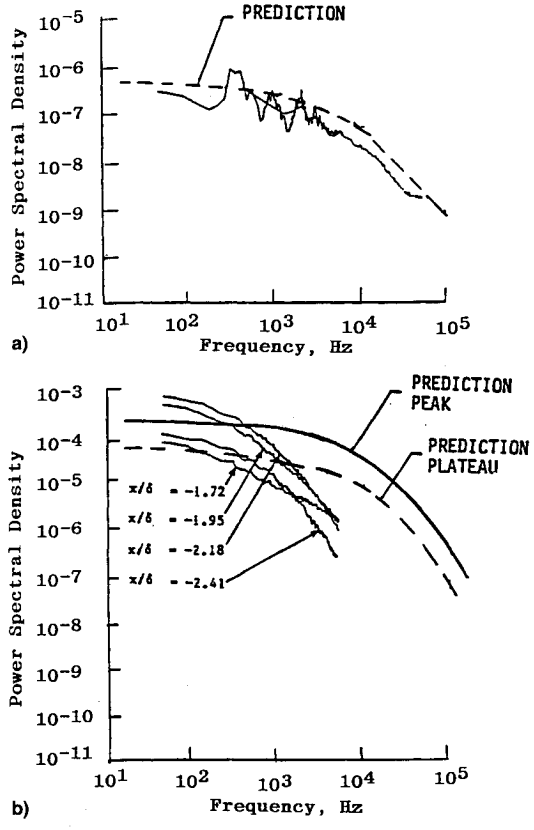

Fig. 8 Comparison of prediction technique to measured power spectral data for a 24-deg compression ramp: a) power spectral distribution of approach flow and b) power spectra in the intermittent region.[22]

Power spectra of swept shock/boundary-layer interactions were measured by Tran et al.[24] at various shock strengths, and are shown in Fig. 9 for a 20-deg shock generator. The measurements were made from the undisturbed flow (no. 1) through the interaction regime; notably at the position of peak rms pressure (no. 2), plateau (no. 3), and second pressure rise (no. 4) levels. The data are not normalized due to the inability to definitize length and velocity scales.

As previously noted, it would be desirable to characterize the normalized power spectra using approach boundary-layer flow parameters leading to the shock/boundary-layer interaction zone. This is a consequence of the ambiguity of definitizing length and velocity scales. Accordingly, the power spectra for attached flow will be used as given by Eq. (4), where k' has been defined as $k' = F_c^{-2\lambda}$ to match the rolloff at high frequency ($f > 2000$ Hz) for attached boundary-layer flow. Moreover, the boundary-layer characteristic parameters of velocity and length will assume the approach flow values designated by the subscript 1. The augmentation in the power spectra due to the low-frequency components will be the sole effect of the normalized rms fluctuating pressure at peak and plateau levels.

Consider the amplitude of the power spectra at low frequencies

$$\phi(f \to 0) \to (4q^2 l/V)F_c^{1.4333}(\tilde{p}/q)^2$$

and restructure the normalized rms pressure in terms of approach flow and peak and/or plateau levels as follows:

$$\left(\frac{\tilde{p}}{q}\right)_{pl} = \frac{\tilde{P}_{W_2}}{P_{W_2}} \cdot \frac{P_{W_2}}{q_2} = \left(\frac{\tilde{P}_{W_1}}{P_{W_1}}\right)\left(\frac{P_{W_2}}{P_{W_1}}\right)_{\max} \frac{P_{W_2}}{q_2} \tag{31}$$

which, in terms of approach flow parameters, can be written as

$$(\tilde{p}/q)_{pl} = (\tilde{P}_{W_1}/q_1)(P_{W_2}/P_{W_1})_{\max}(M_1/M_2)^2 \tag{32}$$

where the Mach number in the plateau region (M_2) is determined from oblique shock relations, namely

$$M_2^2 \sin^2(\theta_s - \alpha) = \frac{(\gamma - 1)M_1^2 \sin^2\theta + 2}{2\gamma M_1^2 \sin^2\theta_s - (\gamma - 1)} \tag{33}$$

The augmented amplitude of the power spectra in the plateau pressure region resulting from the rms fluctuating pressure at low frequency is then described by

$$\phi(f \to 0)_{pl} \to \phi(f \to 0)_{\text{app flow}} \cdot \left[\frac{M_1^2(\gamma + 1)(P_{W_2}/P_{W_1})^2_{\max} \sin^2(\theta_s - \alpha)}{(\gamma - 1)M_1^2 \sin^2\theta_s + 2}\right]^2 \tag{34}$$

where the use of Eq. (24) was made with Eq. (33). Solution to Eq. (34) is made with Eqs. (24), (25), (17), and (7).

For peak power spectra conditions in the intermittent region, the augmentation at low frequencies requires modification of Eq. (28) to include the dynamic pressure. Therefore

$$\left(\frac{\tilde{p}}{q}\right)_{\text{peak}} = \frac{(\tilde{p})_{\text{peak}}}{\tilde{P}_{W_1}} \cdot \frac{\tilde{p}_{W_1}}{q_1} \cdot \frac{q_1}{q_p} = \frac{(\tilde{p})_{\text{peak}}}{\tilde{p}_{W_1}}\left(\frac{\tilde{P}_{W_1}}{q_1}\right)\frac{P_{W_1}}{P_p}\left(\frac{M_1}{M_2}\right) \tag{35}$$

where the dynamic pressure is evaluated at plateau levels (point of separation—actually should be at location of maximum pressure gradient, however this location is difficult to

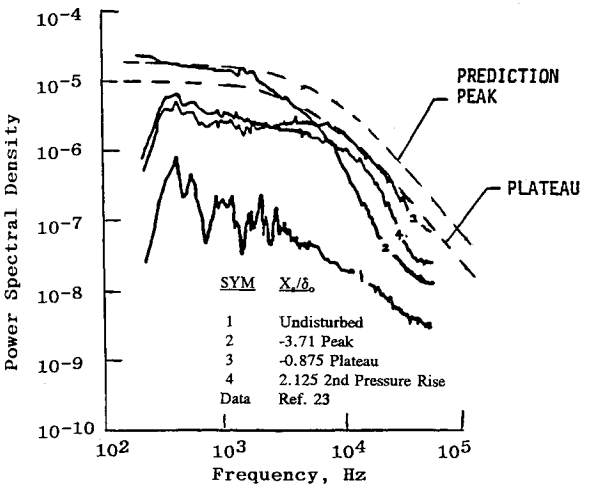

Fig. 9 Comparison of prediction technique to measured power spectral data for a 20-deg fin shock generation.

determine a priori). The amplitude of the augmented peak power spectra becomes

$$\phi(f \to 0)_{\text{peak}} \to \phi(f \to 0)_{\text{app flow}} \left[\frac{(\tilde{p})_{\text{peak}}}{\tilde{p}_{W_1}} \left(\frac{M_1}{M_2} \right)^2 \frac{P_{W_1}}{P_p} \right]^2 \tag{36}$$

where $\tilde{p}_{\text{peak}}/P_{W_1}$ is determined by Eq. (28) for $M \leq 3$, or using Fig. 10 for $M > 3$, M_1/M_2 by Eq. (33), and P_{W_1}/P_p by Eq. (29) or (30).

To describe the spectral distribution of the shock/boundary-layer interactions as shown in Figs. 8 and 9 will require modification to the prediction technique given by Eq. (16). This is a consequence of the rolloff with increasing frequency which displays a steep slope of the energy with interactions when compared to the approach flow characteristics in low-frequency range (<500 Hz). Recall that the roll-off was characterized by the compressibility and heat transfer of the medium in the Strouhal number, i.e., $k' = F_c^{-2\lambda}$. Due to the limitation of data, the characterization of the power spectra over the entire frequency range is considered beyond the scope of the present investigation until a more extensive data base is generated. However, engineering solutions can be made for the interaction behavior over the spectrum using Eqs. (34) and (36) together with Eq. (16).

Figure 8b shows peak and plateau level predictions with the compression corner data of Ref. 22. While the amplitude ($f \to 0$) is reasonably predicted, the spectral distribution is overpredicted in the low-frequency range (as expected). Although not shown, it is expected that the data would tend toward the approach flow at the higher frequencies. Finally, Fig. 9 shows comparisons of the prediction technique to the fin-generated shock/boundary-layer interaction of Ref. 24. It appears that the rolloff characteristics for the three-dimensional-type interactions are more commensurate with attached flow behavior, thereby allowing for a reasonable engineering estimate of the power spectra.

Summary

A technique has been presented that predicts the rms pressure intensity and power spectra in attached, zero pressure gradient turbulent boundary-layer flows on smooth and rough surfaces. The latter surface conditions considers augmentation in the intensity using the rough-to-smooth wall skin-friction ratio. The impact of roughness on the power spectra is due to the skin-friction ratio (i.e., rms pressure) and to a lesser extent on the boundary-layer displacement thickness.

The power intensity (rms pressure) and power spectra for shock/boundary-layer interactions was shown to be related to the shock strength. A modified shock angle was defined in the oblique inviscid pressure relationship that allowed for prediction of the peak and plateau rms pressure levels in the intermittent region. Good agreement for these two rms pressure levels was shown to measured data in the limited test range of Mach number ≤3. Recent data obtained at Mach 5 for both compression ramp and fin-generated interactions appear to correlate with the modified shock angle.

An engineering solution for peak and plateau level pressure interactions appears possible for power spectra magnitude ($f \to 0$). However, the steep slopes and rapid rolloff with the spectra could not be predicted with the attached flow algorithms by using peak and plateau rms pressure levels.

The algorithms developed within are based on a limited data base. Extrapolations of these results to hypersonic conditions to provide design criteria for complex control surface structures should be viewed with caution. Moreover, recent data at Mach 5 suggests the possibility that the rms peak fluctuating pressure could asymptote with compressibility in nonattached flow as was experienced for attached flows. It is believed that the fluid dynamic similarity parameters, together with the attached flow knowledge at hypersonic conditions, allow for first-order design solutions until a more extensive data base can be generated.

Acknowledgments

The author wishes to acknowledge the sponsorship of this work under U.S. Air Force Contract F33615-87-C-3227 entitled, "Thermo-Vibro-Acoustic Loads and Fatigue of Hypersonic Flight Vehicle Structures." The work is monitored by Wright-Patterson Air Force Base-WL/FIBG.

References

[1]Chaump, L. E., Martellucci, A., and Monfort, A., "Aeroacoustic Loads Associated with High Beta Vehicles," Air Force Flight Dynamics Lab., AFFDL-TR-72-138, Wright-Patterson AFB, OH, May 1973.

[2]Laganelli, A. L., Martellucci, A., and Shaw, L. L., "Wall Pressure Fluctuations in Attached Boundary Layer Flow," *AIAA Journal*, Vol. 21, No. 4, 1983, pp. 495–502.

[3]Laganelli, A. L., Christoph, G. H., and Fiore, A. W., "Experimental and Analytical Acoustic Technique to Measure Wall Shear," AIAA Paper 84-0103, Jan. 1984.

[4]Laganelli, A. L., and Scaggs, N. E., "Wallshear Characteristics on Smooth and Rough Surfaces Based on Acoustic Measurement," Air Force Wright Aeronautical Lab., AFWAL TR-85-3114, Wright-Patterson AFB, OH, Jan. 1986.

[5]Laganelli, A. L., and Sontowski, J., "Drag and Aeroacoustic Noise Characteristics Generated by Surfaces Featuring Coupled Roughness and Blowing," American Society of Mechanical Engineers Energy Sources Tech. Conf., FED-VOL II, New Orleans, LA, Feb. 1984.

[6]Settles, G. S., and Dolling, D. S., "Swept Shock Wave/Boundary Layer Interactions," *Tactical Missile Aerodynamics*, Vol. 141, Progress in Astronautics and Aeronautics, AIAA, New York, 1992, pp. 505–574.

[7]Tran, T. F., "An Experimental Investigation of Unsteadiness in Swept Shock Wave/Turbulent Boundary Layer Interactions," Ph.D. Dissertation, Mechanical Engineering Dept., Princeton Univ., Princeton, NJ, March 1987.

[8]Dolling, D. S., and Smith, D. R., "Unsteady Shock-Induced Turbulent Separation in Mach 5 Cylinder Interactions," AIAA Paper 88-0305, Jan. 1988.

[9]Tran, T. T., and Bogdonoff, S. M., "A Study of Unsteadiness of Shock Wave/Turbulent Boundary Layer Interactions from Fluctuating Wall Pressure Measurements," AIAA Paper 87-0552, Jan. 1987.

[10]Dolling, D. S., and Dussauge, J. P., "Fluctuating Wall Pressure Measurements," *A Survey of Measurements and Measuring Techniques in Rapidly Distorted Compressible Turbulent Boundary Layers*, Agardograph, Spring 1988, Chap. 8.

[11]Andreopoulos, J., and Muck, K. C., "Some New Aspects of the Shock Wave Boundary Layer Interaction in Compression Ramp Flows," *Journal of Fluid Mechanics*, Vol. 180, 1987, pp. 405–428.

[12]Dolling, D. S., and Or, C. T., "Unsteadiness of the Shock Wave

Structure in Attached and Separated Compression Ramp Flowfields," *Experiments in Fluids*, Vol. 3, 1985, pp. 24–32.

[13]Schmisseur, J. D., and Dolling, D. S., "Unsteady Separations in Sharp Fin-Induced Shock Wave/Turbulent Boundary Layer Interaction at Mach 5," AIAA Paper 92-0748, Jan. 1992.

[14]Erengil, M. E., and Dolling, D. S., "Effects of Sweepback on the Dynamics of Unsteady Separation in Mach 5 Compression Ramp Interactions," AIAA Paper 92-0430, Jan. 1992.

[15]Dolling, D. S., and Brusniak, L., "Correlation of Separation Shock Motion in a Cylinder Induced Interaction with Pressure Fluctuations Under the Separated Region," AIAA Paper 91-0650, Jan. 1991.

[16]Settles, G. S., and Dolling, D. S., "Swept Shock/Boundary-Layer Interactions-Tutorial and Update," AIAA Paper 90-0375, Jan. 1990.

[17]Laganelli, A. L., and Wolfe, H., "Prediction of Fluctuating Pressure in Attached and Separated Turbulent Boundary Layer Flow," AIAA Paper 89-1064, April 1989.

[18]Lowson, M. V., "Prediction of Boundary Layer Pressure Fluctuations," Air Force Flight Dynamics Lab., AFFDL-TR-67-167, April 1968.

[19]Burton, T. E., "Wall Pressure Fluctuations at Smooth and Rough Surfaces Under Turbulent Boundary Layers with Favorable and Adverse Pressure Gradients," Massachusetts Inst. of Technology, TR 70208-9, Cambridge, MA; see also AD772548.

[20]Blake, W. K., "Turbulent Boundary Layer Wall Pressure Fluctuations on Smooth and Rough Walls," *Journal of Fluid Mechanics*, Vol. 44, Pt. 4, Dec. 1970.

[21]Dolling, D. S., and Murphy, M. T., "Unsteadiness of the Separation Shock Wave Structure in a Supersonic Compression Ramp Flowfield," *AIAA Journal*, Vol. 21, No. 12, 1983, pp. 1628–1634.

[22]Muck, K. C., Dussauge, J. P., and Bogdonoff, S. M., "Structure of the Wall Pressure Fluctuations in a Shock-Induced Separated Turbulent Flow," AIAA Paper 85-0179, Jan. 1985.

[23]Tan, D. K., Tran, T. T., and Bogdonoff, S. M., "Wall Pressure Fluctuations in a 3-D Shock-Wave/Turbulent Boundary Layer Interaction," *AIAA Journal*, Vol. 25, No. 1, 1987, pp. 14–21.

[24]Tran, T. T., Tan, D. K., and Bogdonoff, S. M., "Surface Pressure Fluctuations in a Three-Dimensional Shock Wave Turbulent Boundary Layer Interactions at Various Shock Strengths," AIAA Paper 85-1562, July 1985.

[25]Neumann, R. D., and Hayes, J. R., "Prediction Techniques for the Characteristics of the 3D Shock Wave Turbulent Boundary Layer Interactions," AIAA Paper 77-46, Jan. 1977.

[26]Coe, C. F., Chyu, W. J., and Dods, J. B., "Pressure Fluctuations Underlying Attached and Separated Supersonic Turbulent Boundary Layers and Shock Waves," AIAA Paper 73-996, Oct. 1973.

[27]Nestler, D. E., and Hall, D. W., "Flow Field Separation Approximations for Hypersonic Aerodynamics," Air Force Wright Aeronautical Lab., AFWAL-TR-88-3025, Wright-Patterson AFB, OH, May 1988.

[28]Holden, M. S., "Experimental Studies of Quasi-Two-Dimensional and Three-Dimensional Viscous Interaction Regions Induced by Skewed-Shock and Swept-Shock Boundary-Layer Interaction," AIAA Paper 84-1677, June 1984.

[29]Scuderi, L. F., "Expressions for Predicting 3-D Shock Wave-Turbulent Boundary Layer Interaction Pressures and Heating Rates," AIAA Paper 78-162, Jan. 1978.

[30]Robertson, J. E., "Prediction of In-Flight Fluctuating Pressure Environments Including Protuberance Induced Flow," Wyle Lab., Rept. WR71-10, Huntsville, AL, March 1971.